Available online at www.eccomasproceedia.org
Eccomas Proceedia COMPDYN (2017) 120-141

ECCOMAS
Proceedia

COMPDYN 2017
6th ECCOMAS Thematic Conference on
Computational Methods in Structural Dynamics and Earthquake Engineering
M. Papadrakakis, M. Fragiadakis (eds.)
Rhodes Island, Greece, 15–17 June 2017

EXPERIMENTAL MEASUREMENTS AND NUMERICAL SIMUATION OF NOVEL ANCHORING DEVICES FOR OPEN HOOP FIBER REINFORCING POLYMER STRIPS USED IN THE SHEAR UPGRADE OF R/C T-BEAMS

George C. Manos[1], K. Katakalos[2], G. Mpalaskas[3]

[1] Professor and ex-Director of the Lab. of Strength of Materials and Structures, Aristotle University
e-mail: gcmanos@civil.auth.gr

[2] Dr. Civil Engineer, Research Ass., Lab. of Strength of Materials and Structures, Aristotle University
e-mail: katakaloskostas@gmail.com

[3] Postgraduate student, Lab. of Strength of Materials and Structures, Aristotle University

Keywords: Retrofitting, Reinforced Concrete Frames, Encasement R/C Panels, Jacketing, Soft Ground Floor

Abstract. *Shear strengthening of reinforced concrete (R/C) T-Beams can be achieved by open hoop FRP strips applied externally as transverse reinforcement. Unless these FRP strips are anchored the transfer of tensile forces developing in these strips relies solely on the interface between the FRP sheet and the concrete contact surface. In this case, the delamination (de-bonding) mode of failure of these FRP strips is very likely to occur, disrupting the effective-ness of such a shear strengthening scheme. Consequently, there is need to study both this debonding mode of failure as well as various forms of effective anchoring. For this purpose a number of special unit T-Beam R/C specimens were fabricated employing open hoop FRP strips with or without anchoring. One type of anchoring that was tested is based on a novel anchoring device. It was demonstrated that an anchoring scheme devised by the authors can provide the necessary satisfactory transfer of forces between the FRP strip and the concrete volume of the R/C T-Beam. This used testing arrangement was also numerically simulated employing the exact properties of the materials which were used in the experimental sequence. Two different types of numerical models were studied. The first was without any anchoring device whereas the second the novel anchoring device that was employed during testing was simulated in detail. It can be demonstrated that the used numerical simulation predicts in a satisfactory way both the bearing capacity as well as the mode of failure that was observed in the test specimens with or without the anchoring device.*

Peer-review under responsibility of the organizing committee of COMPDYN 2017.
doi: 10.7712/120117.5412.16891

1 INTRODUCTION

Many reinforced concrete (R/C) structural members need strengthening either because they were built according to old code provisions and do not meet the current design requirements, or because they are damaged after extreme events such as a strong earthquake sequence and they are in need of repair and strengthening (figure 1, [4]). When such a strengthening scheme uses externally bonded FRP layers [1] one of the basic problems is the successful transfer of tensile forces between these polymer sheets and the concrete parts of the structure in order to exploit their high tensile capacity [8] (figure 2). Frequently, it is necessary to introduce an appropriate anchoring scheme in order to prevent premature FRP strip debonding failure in order to exploit successfully the high levels of tensile forces that these FRP layers can withstand and thus meet the strengthening design requirements for the structural members under consideration ([3], [5], [6], [7]). There is a real necessity to develop reliable anchoring details that can accompany such repair and strengthening schemes of R/C structural elements employing multi-layer FRP strips in such a way that the FRP parts together with their anchoring detail can provide a feasible and safe solution for such an application. Specific experimental investigations have been conducted to study this FRP strip debonding type of failure and to investigate means for improvement.

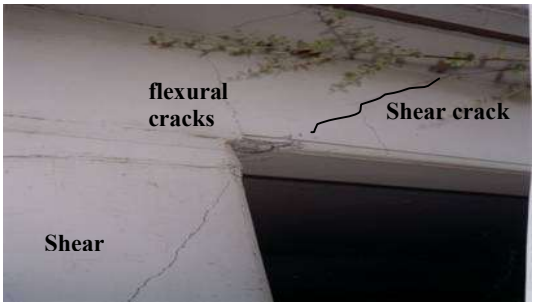

Fig. 1. Damage of T-Beam at the joint with the nearby column (6th story building, Aharnes, Athens earthquake 1995) [4].

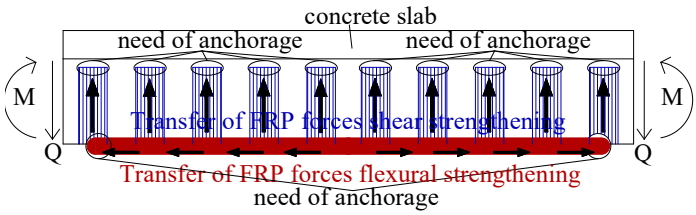

Fig. 2. Flexural and shear retrofitting of a R/C T-Beam by applying FRP strips attached externally on the concrete surface. Need of anchors for the effective force transfer [8].

2 TESTED ANCHORING SCHEMES UNDER MONOTONIC LOAD UTILIZING THE UNIT T-BEAM SPECIMENS

2.1 Experimental setup

Figures 3a to 3d depict the same R/C unit T-Beam specimens that were used during this study. All these specimens have as a basis the same prototype R/C T-Beam shown in figures 4a, 11b, 12a and 12b. All these unit T-Beam specimens represent a slice with a width of approximately 250mm of this double reinforced prototype R/C T-Beam with the same cross-section, materials and structural details. This prototype beam, shown in figures 4a, 11b, 12a and 12b was designed and constructed to be deficient in terms of shear strength thus to be in need of shear strengthening. This shear strengthening was applied by attaching externally open hoop CFRP strips as shown schematically in figures 3b, 3c and 3d (see also figure 12b). Apart from the three shear strengthening schemes shown in figures 3b, 3c and 3d additional alternative shear strengthening schemes employing open hoop carbon FRP (CFRP) and steel FRP (SFRP)

strips were also studied. However, due to space limitations, only the behaviour of shear strengthening schemes linked with the ones shown by figures 3b, 3c and 3d are reported here.

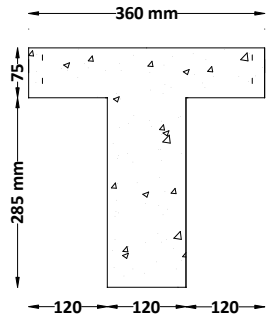

Fig. 3a. R/C T-Beam without an FRP strip

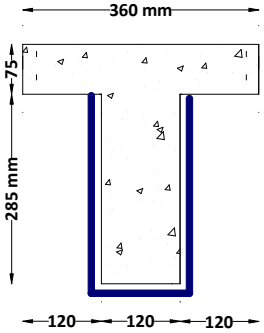

Fig. 3b. R/C T-Beam with an open hoop FRP strip simply attached.

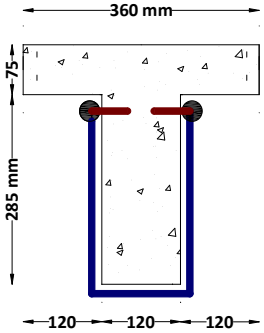

Fig. 3c. Open hoop FRP strip anchored with a mechanical anchor.

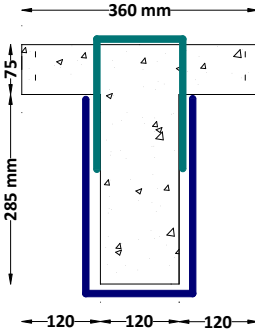

Fig. 3d. Open hoop FRP strip anchored with an FRP anchor.

In all these shear strengthening schemes, shown in figures 3b to 3d, open hoop CFRP strips were employed in an effort not to break the reinforced slab of the T-Beam, apart from drilling relatively small diameter holes. In the first scheme the open hoop CFRP strip was simply attached at the sides and bottom of the R/C T-Beam, as shown in figure 3b, leaving the R/C slab undisturbed [2, 11, 12]. Alternatively in the second scheme, the open hoop CFRP strip was again attached at the sides of the T-Beam also employing side mechanical anchors devised by the authors [3], in the way shown in figure 3c. Finally, in the last scheme (figure 3d), before attaching the open hoop CFRP strip at the sides and bottom of the R/C T-Beam, as was done before (figures 3b and 3c), a CFRP anchor rope, which was specially provided by the FRP suppliers [10], was inserted from the top of the slab through 16mm diameter holes that were drilled for this purpose, as shown in figure 3d. After this CFRP anchor rope is placed in position through these holes its fibers are spread out at the sides of the T-Beam in such a way that this rope becomes flat and obtains a considerable width in order to be attached to the open hoop CFRP strip placed from the bottom of the T-Beam (figure 3d). Epoxy resin is used to both fill the fibers of this CFRP anchor rope as well as to attach these spread rope fibers to the fibers of the open hoop CFRP strip.

Fig. 4a. Prototype R/C T-Beam tested with or without external CFRP strips as shear reinforcement.

Fig. 4b. R/C units T-Beam with a CFRP strip being axially loaded.

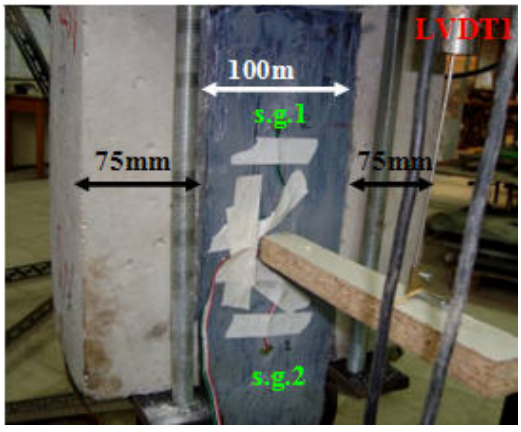

Fig. 4c. Central placement of the CFRP open hoop strip on the R/C unit T-Beam.

The performance of these three shear strengthening schemes depicted in figures 3b, 3c and 3d were initially investigated using the unit T-Beam testing arrangement shown in figures 4b and 4c. As already stated, all these unit T-Beam specimens represent a slice of 250mm width of a double reinforced prototype R/C T-Beam with the same cross-section. The experimental set-up for testing these unit T-Beam specimens is shown in figures 4b and 5.

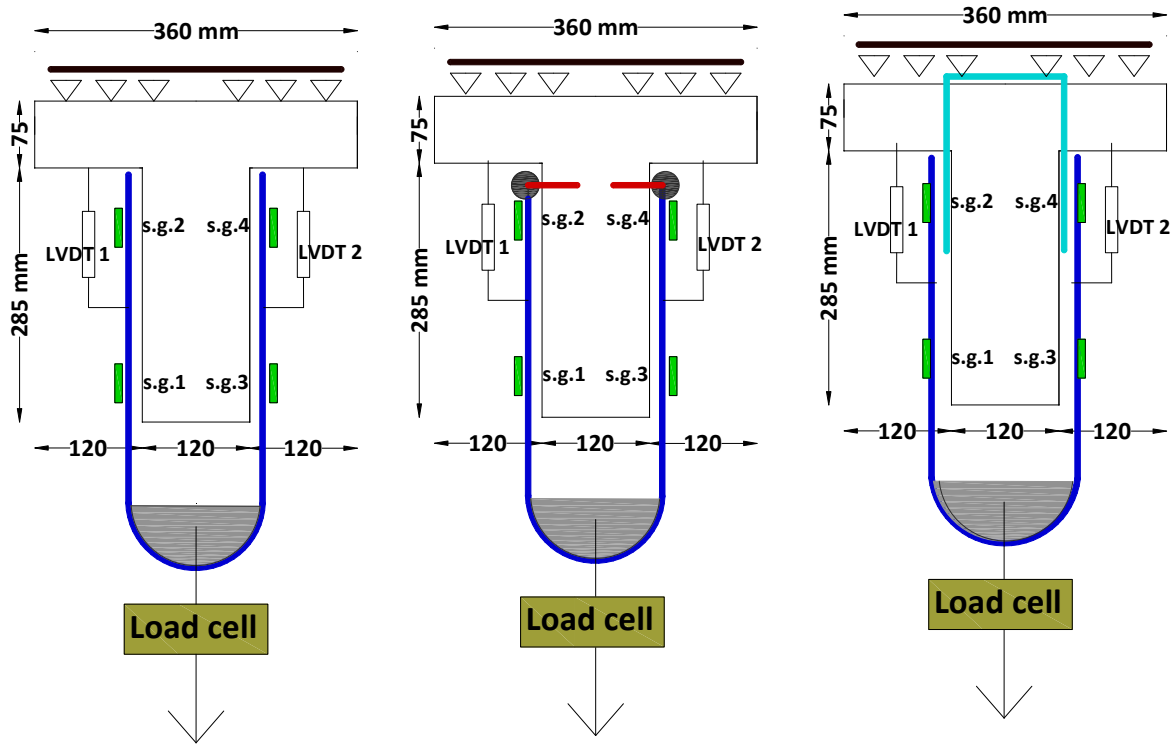

Fig. 5. Testing three different open hoop CFRP strips employing unit T-Beam loading arrangement.

As can bee seen in these figures, each specimen, after the CFRP strip was set in approximately seven days after its attachment, was loaded axially (figures 4b and 5). Instrumentation was provided to monitor the variation of the applied axial load as well as the deformation of the attached CFRP strip in order to record its state of stress as well as the slip of the CFRP from the surface where it was bonded to the volume of the concrete. Four strain gauges (s.g.1 to s.g.4 in figure 5) were put in place, two at each side of the CFRP strip, as indicated in figures 4c and 5. These strain gauges were placed at the axis of symmetry of each strip/specimen at two heights along the bonded surface as shown in these figures. In addition, two displacement transducers were also placed at the axis of symmetry of each specimen in order to record the relative vertical (slip) displacement between the CFRP strip and the underlying concrete surface of the unit T-Beam specimen, which for this level of axial load was considered to be in itself almost non-deformable. Under such axial loading, reproducing in this way the state of stress of open hoop FRP strips applied in prototype T-Beams as external shear reinforcement, the following limit states were expected to occur.

a) The debonding of the FRP from the concrete surface. This is commonly observed for strain/stress levels of the FRP strip relatively well below the limits given by the manufacturers of the FRP materials. The strain/stress levels accompanying this debonding mode of failure continually decrease when one increases the layers of the FRP strip, and consequently its thickness and cross-sectional area, rendering such layer increase totally ineffective unless it is

combined with some type of anchoring. This type of failure is depicted in figure 6a as observed during the current investigation (see also figure 12b).

b) From the preceding discussion it becomes obvious that the debonding mode of failure prevails in almost all cases where an open hoop FRP strip is simply attached without any anchoring. However, the effective anchoring of such an open hoop FRP strip is not easy. Thus the second category of modes of failure includes limit states in which the final debonding and failure of the FRP strip is a result of the interaction between the FRP strip and the used anchoring scheme. In many cases, the employed anchoring scheme is insufficient to withstand the level of axial force that the FRP strip can withstand by itself in ideal axial tension conditions leading to either local failure of parts of the anchoring scheme or local failure of the FRP strip in areas neighbouring the anchor or both. Again, the increase of the layers of the FRP strip, and consequently of its thickness and cross-sectional area, results in a corresponding increase in the demands on the various parts of the anchoring scheme leading them to partial successive failure. This type of failure is depicted in figure 6b as was observed during the current investigation for an anchoring scheme that proved ineffective and is not reported further in this paper.

c) The final mode of failure is a form of tensile failure of the FRP strip. The closer this tensile failure resembles an ideal symmetric axial tensile failure of the FRP strip the higher the axial strain/stress levels that would develop thus resulting in a higher exploitation of the capabilities of the FRP material. This desirable FRP strip performance is observed when the used anchoring scheme is effective in inhibiting any asymmetric local deformation patterns for the axial tensile force levels that correspond to such relatively high strain/stress levels of FRP strip. The final limit state condition is that of the fracture of the FRP strip that is obviously preceded by its debonding. This type of failure is depicted in figure 6c as observed during the current investigation for the anchoring scheme of figure 3c which proved to be effective in withstanding the level of forces that developed at the FRP strip up to its tensile fracture. Again, the effectiveness of an anchoring scheme is directly linked with the corresponding number of layers of the FRP strip that it tries to anchor. For a given effective anchoring scheme linked with an FRP strip having a given number of layers, a successive increase in the numbers of layers will eventually lead to the failure of the anchoring scheme, unless it is properly redesigned.

Fig. 6a. Debonding mode of failure

Fig. 6b. Failure of the anchoring scheme accompanied with debonding

Fig. 6c. Tensile failure of the FRP strip

2.2 Measured response of unit T-Beams employing open hoop CFRP strips with no anchors

Figures 7a and 7b depict the measured displacement and CFRP strain response versus the applied axial load, respectively, as was recorded for a unit T-Beam specimen, named CSN1, that had a single layer CFRP strip simply attached without the use of any anchoring device (Figures 3b, 4c and 5). As can be seen in figure 7a the slip-deformation starts at the side that is recorded by LVDT1 for a relatively lower value of the applied axial load than for the corresponding slip that is recorded by LVDT2. The strains of the FRP strip at this side (LVDT1) are recorded by strain gauges s.g.1 and s.g.2 whereas for the side where the slip is recorded by LVDT2 the corresponding strain gauges are s.g.3 and s.g.4. Strain gauges s.g.1 and s.g.3 are near the bottom fiber of the T-Beam whereas strain gauges s.g.2 and s.g.4 are at the end of the FRP strip near the slab of the T-Beam cross-section. As can be seen from figure 7b strain gauges s.g.1 and s.g.3, which are located near the bottom fiber of the T-Beam, start recording considerable axial strains for relatively lower values of applied axial load than strain gauges s.g.2 and s.g.4, which record considerable strains when the bond- slip has reached levels near the limit-state that is next followed by the maximum load and subsequently the debonding mode of failure. Utilizing all these strain measurements together with the CFRP cross-section and the measured Young's modulus of the CFRP material, which was obtained from independent special tensile tests, an indirect axial load value is found that is also plotted in figure 7a against the LVDT1 measured slip displacement. As can be seen, reasonably good agreement is observed between the axial load value as measured directly through the load cell and the corresponding axial load value found indirectly through these axial CFRP strain measurements.

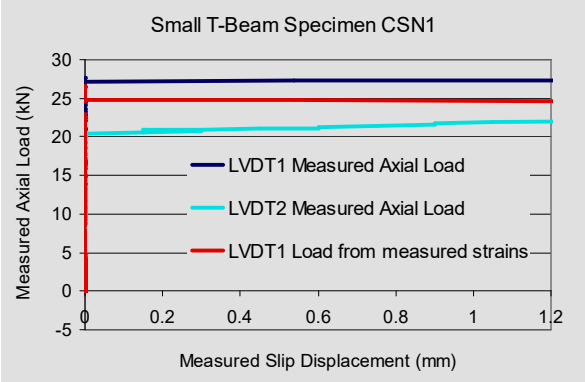

Fig. 7a. Measured slip displacements. Specimen CSN1

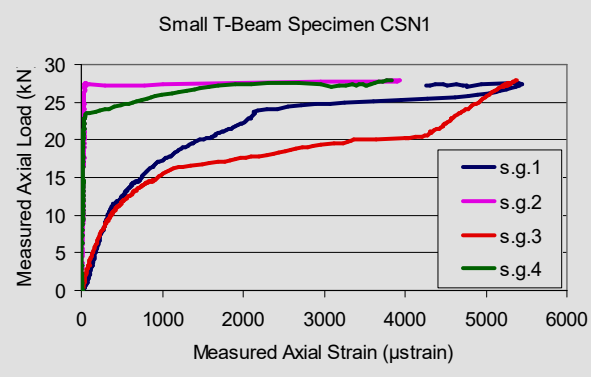

Fig. 7b. Measured FRP strip axial strains.

2.2. Measured response from unit T-Beams with CFRP strips employed anchors

Figures 8a and 8b depict the measured slip displacement and CFRP strain response versus the applied axial load, respectively, as was recorded for a unit T-Beam specimen, named CSP2s, that had a two-layer CFRP strip attached with the use of the anchoring scheme of Figure 3c (see also figures 4c and 5, [3]). The results plotted in figures 8a and 8b were obtained from a third loading sequence applied to this unit T-Beam specimen being preceded by two similar loading sequences. During the 1st loading sequence the maximum axial load value was equal to 85KN; during the 2nd loading sequence the maximum axial load reached the value of 95KN. Finally, during the 3rd loading sequence the maximum axial load reached approxi-

mately 115KN and was accompanied by the fracture of the CFRP strip. Further results from the 1st and 2nd loading sequences are not shown here.

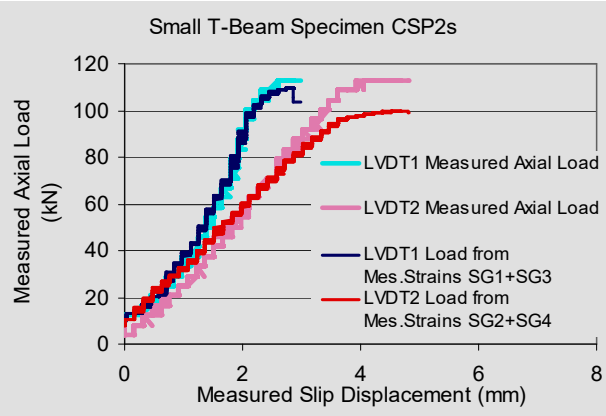

Fig. 8a. Measured slip displacements. Specimen CSP2s

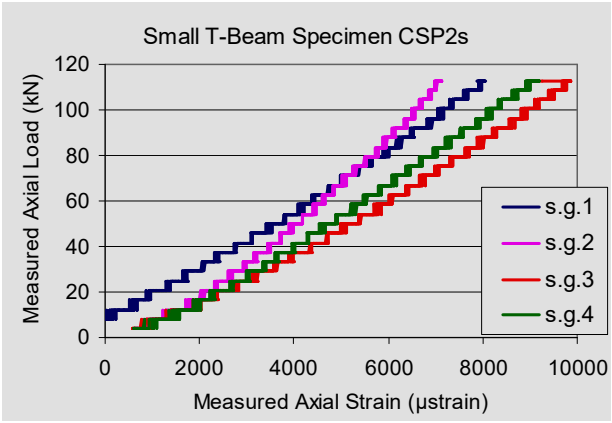

Fig. 8b. Measured FRP strip axial strains.

As was done before for specimen CSN1, utilizing all the relevant strain measurements, the CFRP cross-section and the measured Young's modulus of the CFRP material indirect axial load values were found that are also plotted in figure 8a. One of these indirect axial load values is based on the FRP strip strain measurements near the bottom of the T-beam (s.g.1 and s.g.3) and is plotted against the LVDT1 measured slip displacement. The second indirect axial load value is based on the FRP strip strain measurements near the slab of the T-Beam (s.g.2 and s.g.4) and is plotted against the LVDT2 measured slip displacement. As can be seen in figure 8a reasonably good agreement can be observed between the axial load value measured directly through the load cell and the indirect load values based on these axial strain measurements of the CFRP strip. The maximum indirect load values based on either the bottom or the top T-Beam locations are quite close to each other as well as to the direct axial load value. This fact supports the previously mentioned hypothesis which states that at the limit state the debonding of the CFRP strip has already occurred; the total axial force is resisted during this limit state only by the anchors. The measured CFRP strip strain values linked with the debonding, listed in Table 1, also support this hypothesis. As can be seen in figure 8b, the maximum strains, measured by s.g.1 and s.g.2, reach values of 10000μstrains. The variation of these measured strains with the applied axial load is almost linear. Moreover, these measured strain values are almost the same for all four locations; this indicates again that the CFRP strip is debonded during the first two loading sequences and the transfer of the axial force during the third and final loading sequence is achieved solely through the used anchors. Because of the high values of the measured CFRP axial strains and the fact that the employed CFRP strip had two layers, the maximum amplitude of the applied axial force reached a maximum level of 114.71KN. This is almost three times the corresponding maximum axial load value for single layer specimen CSN1 that did not employ any anchor and failed by debonding. This large increase of the transferred axial load could be achieved through the employed anchoring scheme that performed in a very satisfactory way resulting in axial strains for the CFRP strip that are considerably closer to the maximum material strain values given by the manufacturer (ideally 18000μstrains) or observed during the specified axial tensile test performed at the laboratory to obtain the material properties (10000μstrains). For both specimens CSN1 and CSP2s the bond surface of the concrete volume was not treated in any special way apart from being thoroughly cleaned. The present investigation was supplemented with two more specimens. The first specimen is named CRN1 and was identical to CSN1; the second specimen is

named CRP2s and was identical to CRP2s. The only difference introduced between these specimens is that for specimens CRN1 and CRP2s the bond surface of the concrete volume was treated by a special hammer in order to become rough as well as being thoroughly cleaned. The obtained summary results of all these four specimens are listed in table 1. As can be seen from the relevant axial strain and axial load values listed in table 1, the special treatment of the bond surface, as expected, resulted in a considerable increase in the level of the maximum axial load that can be transferred from the CFRP strip to the concrete volume through the bond surface. On the contrary, in the case of employing the efficient anchoring scheme of figure 3c the influence of the bond surface was immaterial. As explained before, this is because when an efficient anchoring scheme is employed the transfer of axial force at the limit state is achieved solely through the used anchoring scheme with the debonding already occurring at a preceding stage without affecting the CFRP strip's final performance.

Table 1. Results of unit T-Beam specimens with open hoop CFRP strips with and without the use of anchors.

Specimen Code Name	Maximum measured Axial Load (kN)	Maximum measured FRP strip axial strain values s.g.1-3 (μstrain)	Axial Load (kN) Linked with the FRP strip debonding		Failure mode / Axial load (kN) resulting from the measured FRP axial strains
			s.g.1-2	s.g.3-4	
CSN1* single CFRP layer without anchor	27,94	5670	27,19	20,47	Debonding / 34.17
CRN1** single CFRP layer without anchor	42,67	7114	36,13	33,60	Debonding / 42.87
CSP2s* CFRP with two layers and anchoring of figure 3c	113,0	9518	27,07	34,21	Fracture of FRP / 114.71
CRP2s** CFRP with two layers and anchoring of figure 3c	102,7	8689	41,68	37,86	Fracture of FRP / 104.72

Each CFRP layer had a thickness of 0.131mm, a width of 100mm and a Young's modulus equal to 234GPa.

* No special treatment of the bond surface apart from careful cleaning.

** The bond surface was made rough with a special hammer.

2.3 Response from unit T-Beams with open hoop CFRP strips employing CFRP anchor ropes

In this section the measured response was obtained from the last anchoring scheme being investigated (figure 9a, [10]). This time, before attaching the open hoop CFRP strip at the sides and bottom of the R/C beam, a CFRP anchor rope is inserted from the top through 16mm diameter holes that are drilled in the R/C slab of the T-Beam for this purpose. The effective cross-sectional area of this CFRP rope is equal to 33.1mm2 and the Young's modulus equal to 240GPa. After this CFRP anchor rope has been placed in position through these holes its fibers are spread at the sides of the beam in a way that this rope becomes flat and obtains a considerable width in order to be attached to the single layer open hoop CFRP strip (with an effective cross-sectional area of 13.1mm2), which is put in place from the bottom of the T-Beam. Epoxy resin is used to both fill the fibers of this CFRP rope as well as to attach these spread rope fibers to the fibers of the open hoop CFRP strip. This anchoring scheme was stud-

ied in two different ways. First one anchor rope was used with its axis located at the mid-axis of the width of the open hoop CFRP strip (specimens with the code name SW600C/1 No1, No2 and No3, Table 2). Alternatively, two such anchor ropes were placed side-by side along the width of the open hoop CFRP strip (specimens with the code name SW600C/2 No1, No2, No3 and No4, Table 2).

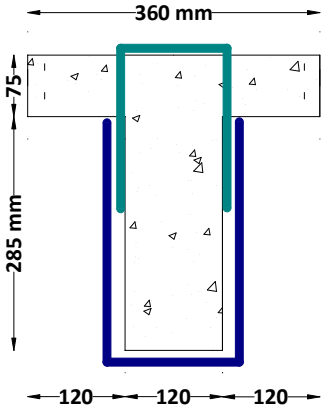

Fig. 9a. R/C T-Beam with an attached open hoop FRP strip anchored with an FRP anchor

Fig. 9b. Mode of failure of specimen SW600C/1 No 1. Fracture of the CFRP rope.

Fig. 9c. Mode of failure of specimen SW600C/1 No 1. Fracture of the CFRP rope.

As can be seen in table 2, when one CFRP rope was used in the anchoring scheme of the 1 layer open hoop CFRP strip the observed failure was mainly at this anchor rope (see figure 9b). On the contrary, when two CFRP anchor ropes were used to anchor the open hoop CFRP strips their tensile capacity led to an effective anchoring scheme leading the tensile fracture of the single layer CFRP strip (figure 9c). As can be seen from the obtained axial load response listed in table 2, when one CFRP anchor rope is used the standard deviation of the obtained values is 4.538KN from an average axial load value of 66.12KN (6.9%). When the same processing is employed for the measured response of the specimens with two CFRP anchor ropes then the standard deviation of the obtained axial load response values, listed in table 2, is 19.576KN from an average axial load value of 86.12KN (22.7%). Consequently, due to this relatively large standard deviation value for the observed measured axial load when two CFRP anchor ropes are employed, it can be concluded that a reduced reliability can be expected in achieving the desired shear capacity when employing a relatively large number of anchor ropes. Moreover, it can also be concluded that this technique is in need of further research. In order to have a direct measurement of the tensile capacity of either the CFRP strip itself or the CFRP anchor rope when in position extra unit T-Beam specimens were constructed whereby the CFRP strip (specimens ref-1 and ref-2, figures 10a and 10b) and the CFRP rope (specimens SWFX No1, No2 and No3, figures 10c and 10d) were accommodated in a close hoop formation and were subjected to the same loading arrangement depicted in figure 5. The obtained results are listed in table 3. As can be seen from the axial load response, listed in table 3, the standard deviation of the obtained values for the closed hoop CFRP anchor rope is 4.208KN from an average axial load value of 70.787KN (5.9%) whereas for the closed hoop CFRP strip the standard deviation is 18.427KN from an average axial load value of 85.63KN (21.52%). Even with this degree of uncertainty, the obtained mode of failure of the open hoop CFRP strip specimens (85.63KN) having one CFRP anchor rope (70.78KN), whereby the fracture of the anchor rope was observed (Table 2 and figure 9b), is partly explained. Similarly, the obtained mode of failure of the open hoop CFRP strip speci-

mens (85.63KN) having two CFRP anchor ropes (upper limit =2*70.78KN), whereby the fracture of the CFRP strip was observed (Table 2 and figure 9c), can again be partly explained.

Table 2. Measured tensile capacity of open hoop CFRP strips anchored with CFRP ropes.

Code name of Specimen	Total Measured axial load (KN)	1 layer CFRP strip Cross-section Area A1=33.1mm^2	CFRP Anchor Rope Cross-section Area A2=28.0mm^2	Measured strain average from both sides of the CFRP strip (µstrain)	Mode of failure
SW600C/1 No 1	60.88	Open hoop	1 rope	3900	Fracture of anchor rope at upper corner
SW600C/1 No 2	68.76	Open hoop	1 rope	4400	Delamination of FRP strips from anchor
SW600C/1 No 3	68.72	Open hoop	1 rope	4400	Fracture of anchor rope at upper corner
SW600C/2 No 1	79.46	Open hoop	2 ropes	5200	Fracture of FRP strip
SW600C/2 No 2	97.18	Open hoop	2 ropes	6400	Fracture of FRP strip
SW600C/2 No 3	61.86	Open hoop	2 ropes	4200	Fracture of FRP strip
SW600C/2 No 4	105.98	Open hoop	2 ropes	5300	Fracture of FRP strip

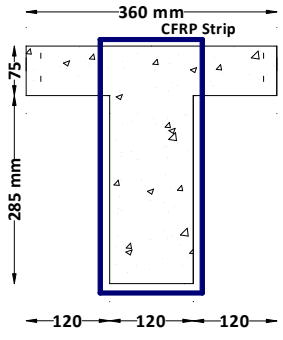

Fig. 10a. Unit T-Beam specimens CFRP strip Ref-1 and Ref-2.

Fig. 10b. Failure mode of specimen CFRP strip Ref-1

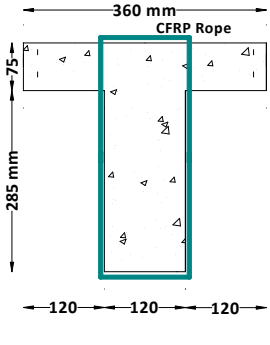

Fig. 10c. Unit T-Beam specimens CFRP Rope SWFX No1, No2 and No3

Fig. 10d. Failure mode of specimen CFRP Rope SWFX No 2

Table 3. Measured tensile capacity of either closed hoop CFRP strips or closed hoop CFRP anchor ropes.

Code name of Specimen	Total Measured axial load (KN)	1 layer CFRP strip Cross-section Area A1=33.1mm^2	CFRP Anchor Rope Cross-section Area A2=28.0mm^2	Measured strain average from both sides of the CFRP strip (μstrain)	Mode of failure
CFRP Strip Ref-1	98.66	Closed hoop	No	6600	Fracture of FRP strip
CFRP Strip Ref-2	72.60	Closed hoop	No	5100	Fracture of FRP strip
CFRP Rope SWFX No 1	69.08	-	Closed hoop anchor rope	-	Fracture of anchor rope
CFRP Rope SWFX No 2	75.58	-	Closed hoop anchor rope	-	Fracture of anchor rope
CFRP Rope SWFX No 3	67.70	-	Closed hoop anchor rope	-	Fracture of anchor rope

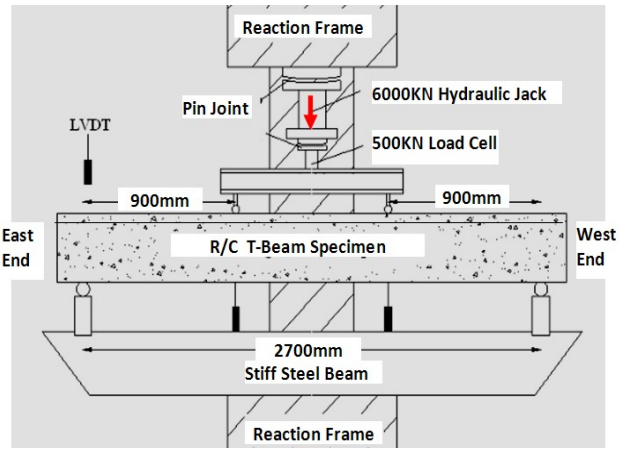

Fig. 11a. Loading arrangement for the prototype T-Beam

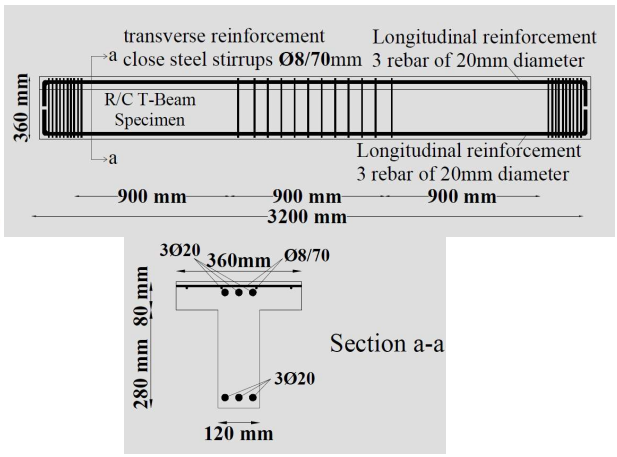

Fig. 11b. Structural details of the T-Beam

3 PROTOTYPE R/C T-BEAM IN NEED OF SHEAR STRENGTHENING.

In this section two of the shear strengthening schemes that were studied before using unit T-Beam specimens are applied to a prototype R/C T-Beam. This T-Beam was designed and constructed to be in need of shear strengthening. Its clear span was equal to 2700mm and was subjected to a four-point bending loading arrangement, as depicted in figure 11a. The applied total vertical load was measured by a load cell and the vertical deflections were recorded near mid-span by two displacement transducers. The central vertical load was applied through a stiff steel girder at two points located 900mm from the two end vertical supports. This T-

Beam had longitudinal reinforcement of 6 reinforcing bars of 20mm diameter that were placed near the top and bottom fiber of the beam (3 at the top and 3 at the bottom, as shown in figure 11b). These steel re-bars had nominal yield stress equal to 500MPa and actual yield stress 531MPa. The concrete compressive strength was found to be equal to 23MPa. The left and right parts of this beam, between the East and West supports and the loading points, has no transverse steel reinforcement intentionally so that the shear mode of failure would prevail. The central part of the beam between the loading points had closed steel stirrups with a diameter of 8mm placed every 70mm intervals in order to prohibit the premature compressive failure of this part of the beam from flexure (figure 11b). Initially, this T-Beam specimen was loaded at its virgin state till the shear limit-state was reached with the appearance of shear cracking patterns at the East and West parts (figure 12a) for a maximum shear force value equal to 57.39KN. Next, a shear strengthening scheme was applied by employing the external application of open hoop CFRP strips. At the West part four (4) 3-layer open hoop CFRP strips were employed (figure 12b) having 0.131mm thickness, 100mm width and spaced at 200mm intervals measured form their center line. These West part CFRP strips employed the anchor scheme of figure 3c. At the East part four (4) 1-layer open hoop CFRP strips were employed instead without any anchors (figure 3b) having 0.131mm thickness and 100mm width and similarly spaced at 200mm intervals measured form their center line. This was done in order to study the debonding mode of failure for the CFRP strips attached at this part. The same loading arrangement was used that this time resulted, as expected, in the debonding mode of failure of the West side unanchored CFRP strips as shown in figure 13 for a shear force equal to 166.77KN. This shear force value is more than three times larger than the shear capacity of the un-strengthened virgin T-Beam. The variation of the applied shear force versus the vertical deflection of the virgin and the strengthened with this 1st shear strengthening scheme T-Beam is depicted in figure 14. It is important to underline that the West part of this T-Beam, although subjected to the same shear force level as the East part, did not show signs of any distress. This is due to the presence of the effective anchors that accompanied the open hoop CFRP strips at this location. The design of this FRP anchoring scheme was facilitated by special designed software [6] as well as valid numerical simulations [9]. Next, the same T-Beam is currently being tested with the CFRP anchor scheme shown in figures 3d and 9a.

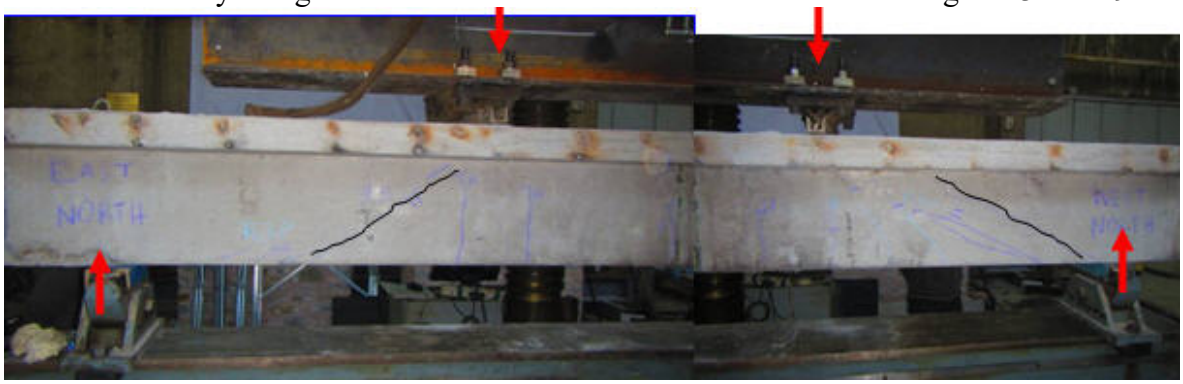

Fig. 12a. Virgin T-Beam that reached a shear limit state under four-point bending

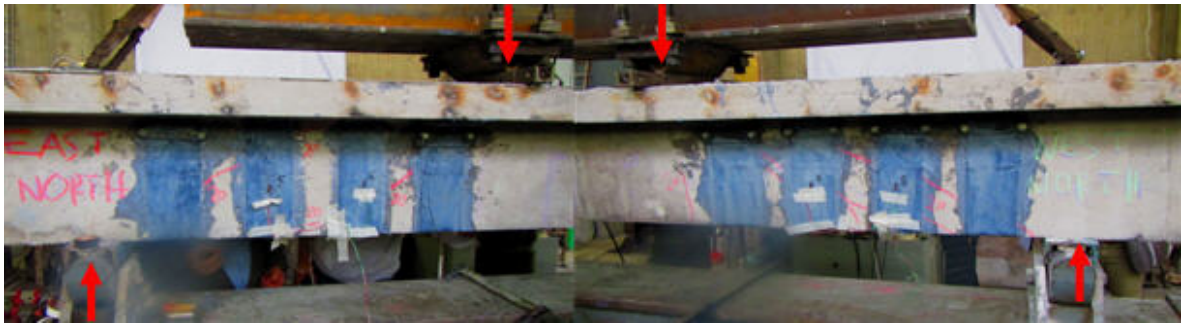

Fig. 12b. T-Beam with the 1st shear strengthening scheme under four-point bending (see also figures 3b and 3c).

Fig. 13. Debonding of the open hoop CFRP strips at the East part of the T-Beam

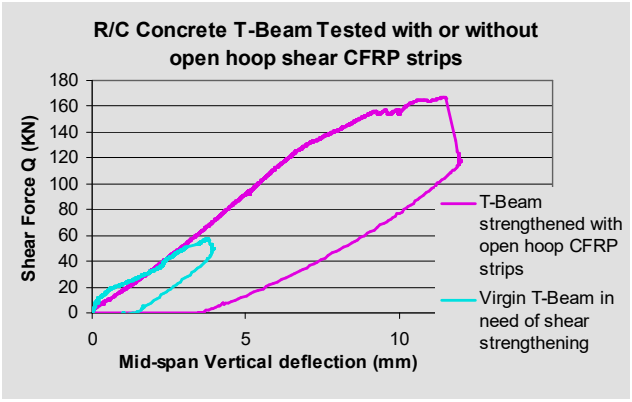

Fig. 14. Variation of the applied shear force versus the vertical deflection of the virgin and the strengthened T-Beam

4 NUMERICAL SIMULATION

The general purpose FE software ABAQUS (Hibbitt et al. [13]) was employed to generate FE models to simulate numerically the structural response of the previously described unit concrete T-beams strengthened with externally attached FRP sheets. The generated models were validated against the respective experimental results. The aim of this part of the study is to generate reliable FE models that can be utilized to enhance the understanding of the fundamental structural response of the FRP shear strengthening scheme of R/C beams with and without anchorage devices and hence optimize the anchorage device design (see Manos et al. 2014, [9]).

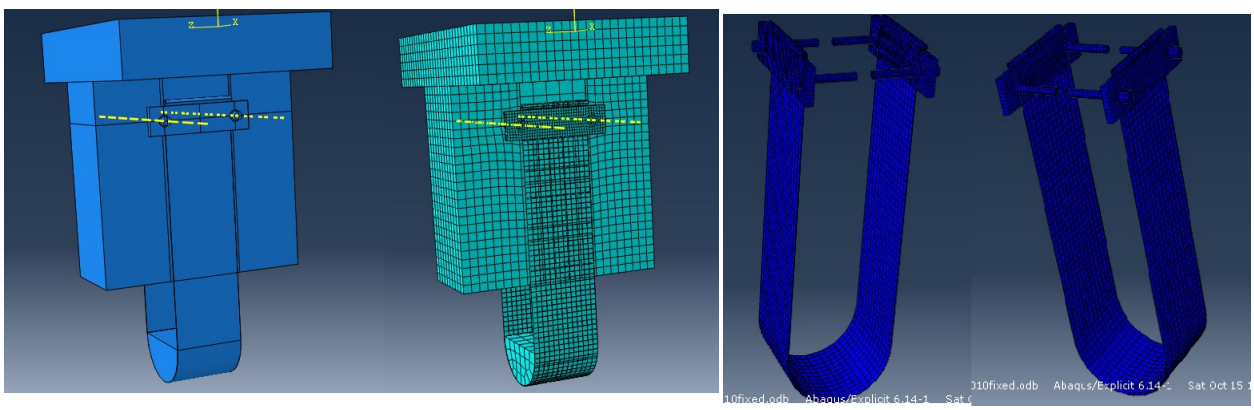

Fig. 15a. Numerical model of unit T-beam with anchored FRP sheets

Fig. 15b. Detail of the numerical model of the anchored FRP sheets

4.1 Modeling assumptions

The mean measured specimen geometries were utilized to simulate the test specimens. The full 3D geometry of the unit T-beam concrete volume and the steel plates employed for the anchorage of the FRP was modeled with 3-D brick-type F.E. elements, whilst the FRP sheets were idealized as planar F.E. elements and their actual thickness was utilized as a section property (see figures 15a and 15b). The bolts were assumed cylindrical with a diameter equal to the equivalent diameter corresponding to the net bolt area (i.e. the threaded part of the bolts was not explicitly modeled). A further idealization pertinent to the bolt assembly simulation is the assumption that the bolt hole diameter of the steel plate is equal to the assumed bolt diameter (i.e. the clearance has not been accounted for).

The load was applied incrementally as prescribed displacement on a steel semi-cylindrical block that was placed within the FRP sheets, which formed a loop of the same geometry at the lower part of each specimen (see figure 5). During testing the load was applied at this steel semi-cylindrical block trough a test machine and was measured by a load cell, as shown in figure 5. In the numerical simulation, the loading was applied iteratively utilizing a smooth amplitude curve available in ABAQUS. Restraint of the structure in the direction of the prescribed displacement was provided by fixing the upper surface of the numerical model of the unit T-beam as shown in figure 16. A dynamic explicit analysis was performed.

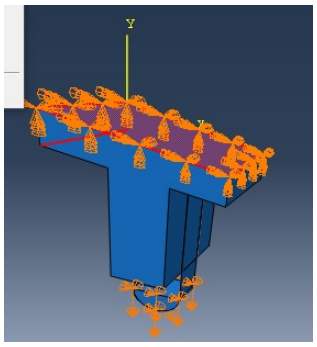

Fig. 16. T-Beam loading and boundary conditions

The sum of the reaction forces in the y direction yields a reaction Ry that corresponds to the total applied load. The contact between the various parts of the model (steel bolts, steel plates and concrete volume) was explicitly modeled and a friction coefficient equal to 0.3 was assumed for tangential contact behaviour except for the contact between the concrete beam and the loading/reaction plates which was assumed frictionless. Moreover, in order to reduce computational cost, the actual detail of the steel rod of the anchoring device through which load is transferred from the FRP strips to the concrete volume through the steel plate was somewhat simplified; towards this end, the displacements of the FRP's edge were constrained to be equal to the respective displacements of the steel plate's mid plane for the numerical representation of the anchoring device. The interface between the FRP and the concrete was simulated as a cohesive zone endowed with a suitable traction separation response. More details can be found in the work by Manos et al. The present numerical investigation dealt with both with the case of unanchored FRP sheets (see detail in figure 3b) as well as with the case whereby the FRP sheets were anchored at the sides of the unit T-beam (see detail in figure 3c). In the former case, the numerical simulation of the anchor steel plate and bolts were obviously omitted and the numerical behaviour was dictated from the bonding / debonding of the FRP sheets from the sides of the unit T-beam, as is explained in the following.

4.2 Numerical simulation of the unanchored FRP strips

When investigating numerically the behaviour of the FRP strips simply bonded on the sides of the unit T-beam specimen without anchors it becomes apparent that such a behaviour is governed by the mechanical properties that are assigned to the specific contact surface between

the FRP sheet and the two sides of the unit T-beam. As already mentioned the interface between the FRP sheet and the concrete volume was simulated as a cohesive zone endowed with a suitable traction separation response. The tested specimens of the unit T-beams without anchor bolts had contact surfaces of two different types. The first type belongs to those unit T-beam specimens left with a relatively "***smooth***" surface, as resulted from the removal of the formwork without any further treatment before the FRP strips were bonded with the help of the resin. The second type belongs to those unit T-beam specimens where this contact surface was roughened with the help of a special hammer ("***rough***"). It was necessary to assign a different value of shear strength to the cohesive elements that simulated numerically this bond contact area between the FRP sheets and the unit T-beam sides. This was done in the following way. From previous research on the debonding of FRP strips from concrete surface it was recommended to adopt as shear strength of this contact interface the tensile strength of the concrete volume. This is because the shear strength of the resin has a much higher value than the tensile strength of the concrete. Thus, the actual debonding mode of failure materializes as a tensile failure of a concrete layer just beneath this contact interface. This recommendation is adopted by design procedures [ ] and it will also be followed here. For the tested unit T-beam specimens the average compressive strength of the concrete was found equal to 20MPa through compression tests of four concrete cylinders, 300mm high with 150mm diameter, which were cast with the same mix and at the same time as the unit T-beam specimens. The tensile strength was not determined through testing but is derived indirectly from this compressive strength, following procedures that are well established from past research. The British Code of practice BS 8007:1987 recommends the following expression for obtaining the tensile concrete strength f_t:

$$f_t = 0.12 * (f'_c)^{\wedge 0.7} \qquad \textit{(Eq. 1)}$$

f'_c in this expression is the cubic compressive strength (in megapascals).
It is also established from past research that the cylindrical compressive strength f_c is approximately equal to 85% of the cubic compressive strength f'_c . Based on these the direct tensile strength of the unit T-beam concrete is found equal to 1.11MPa

Alternatively, the following expression is also recommended:

$$^{s}f_t = \boldsymbol{k} * (f_c)^{\wedge 0.7} \qquad \textit{(Eq. 2)}$$

$^{s}f_t$ represents the tensile splitting strength. The coefficient ***k*** takes values in the range from 0.2 to 0.3); f_c is the compressive strength determined from cylinders (in megapascals).
Based on *Eq. 2* as well as on the relationship between the direct tensile strength and the tensile splitting strength ($f_t = 0.7 * {}^{s}f_t$) the resulting values for the direct tensile strength for the tested unit T-beam specimens is found equal to 1.14MPa or 1.71MPa, for ***k*** values equal to either 0.2 or 0.3, respectively.

All the obtained results for the direct tension strength of the concrete and consequently the shear strength of the contact interface are listed in the following table 4. In the same table the shear strength values that result in the best approximation of the measured unit T-beam capacity when these values are assigned as shear strength values of the cohesive elements employed in the numerical simulation, as previously described. This is done for both the "***smooth***" as well as the "***rough***" contact interface unit T-beam specimens.

Table 4. Direct tensile strength of unit T-beam concrete and shear strength assigned as to the cohesive elements of the numerical simulation

Direct tensile strength of unit T-beam concrete (MPa)			shear strength assigned as to the cohesive elements of the numerical simulation (MPa)	
Eq. 1	*Eq. 2* ***k****=0.2*	*Eq. 2* ***k****=0.3*	"***smooth***" contact surface	"***rough***" contact surface
1.11	1.14	1.71	0.6	1.5

As can be seen from the values listed in table 4, the shear strength value assigned to the cohesive elements of 'rough' specimens numerical simulation is well within the range of concrete tensile strength values obtained as described before. On the contrary, the shear strength value assigned to the cohesive elements of 'smooth' specimens numerical simulation is much smaller; consequently, if the numerical prediction of the behaviour of the 'smooth' specimens would have been based on the tensile strength values of either Eq. 1 or Eq. 2 it would have resulted to approximately two (2) or three (3) times larger capacities for these smooth specimens than the ones measured. From these findings the following important conclusions can be drawn:

1. It is non-conservative to base the estimate of the bearing capacity of bonded FRP strips on concrete surface on the direct tensile strength of concrete, unless the contact surface of the concrete is properly treated prior to bonding the FRP strips.
2. Because the debonding mode of failure leads to a brittle respond is wiser to adopt a higher value of safety factor than it is the case of anchored FRP strips.

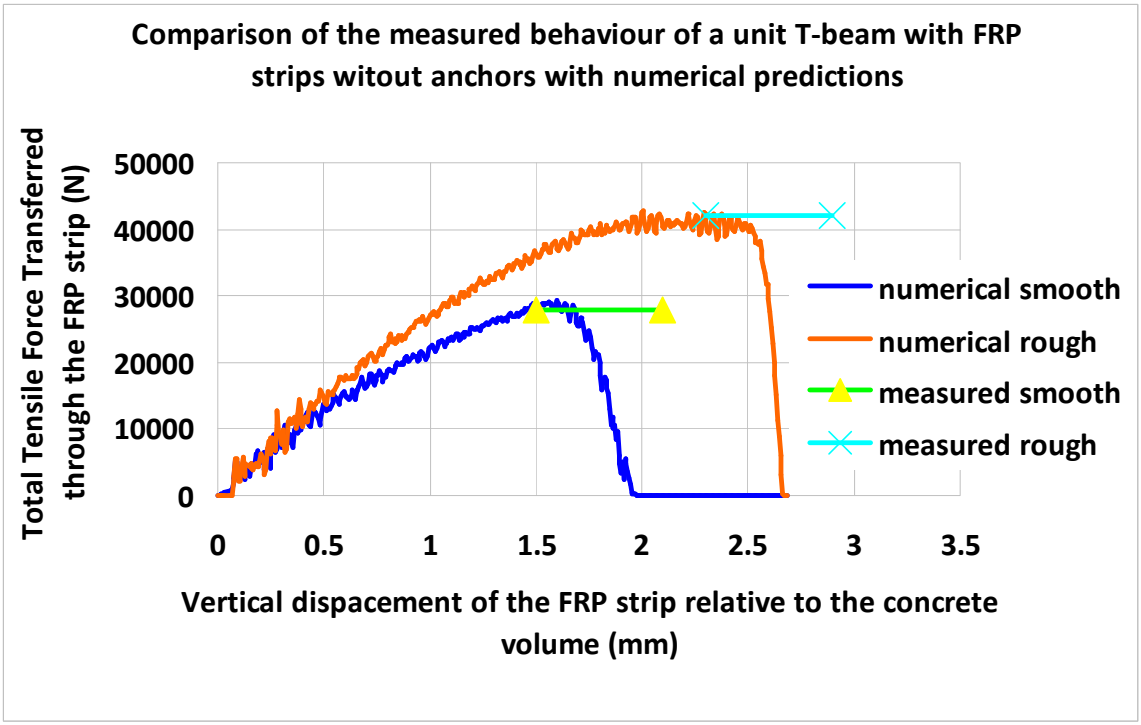

Fig. 16. Comparison of the measured capacity of a unit T-beam specimen with FRP strips being simply bonded without anchors with numerical predictions

Figure 16 depicts the numerically predicted load displacement response of a unit T-beam specimen without anchors with either "smooth" or "rough" contact surface. In the same figure the values of the bearing capacity measured during testing of the corresponding specimens is also indicated. These numerical predictions were obtained assigning shear strength values listed in table 4, as already discussed.

In figure 17 the numerically predicted state of stress (MPa) for the FRP strip, for the cohesive interface and for the concrete block are shown. This is done for two time steps of the loading process. The first that is depicted in the upper row of this figure represents the state of stress at the beginning of the loading sequence whereas the lower row corresponds to the state of stress near the completion (80%) of the loading process before the maximum load is reached. The far left part of this figure represents the state of stress of the FRP strip whereas the mid part that of the cohesive interface. The far right part of this figure represents the state of stress of the concrete block. As can be seen figure 17, an increase in the amplitude of the load results in the spreading of the stressed part of the FRP strip from the bottom to the top. The same trend can also be seen developing at the cohesive interface as well as at the concrete block. The final development of this process results in partial debonding of the FRP strip from the lower part of the concrete block and the concentration of the transfer of force to its upper part through mainly the upper part of the cohesive interface and the corresponding volume of the concrete block, with the FRP strip almost uniformly stressed along its height. This development has as its final stage the complete debonding of the FRP strip and the failure in the transfer of force from the FRP to the concrete block. This numerical process is in good agreement with measurements and observations during tests (see figure 7b).

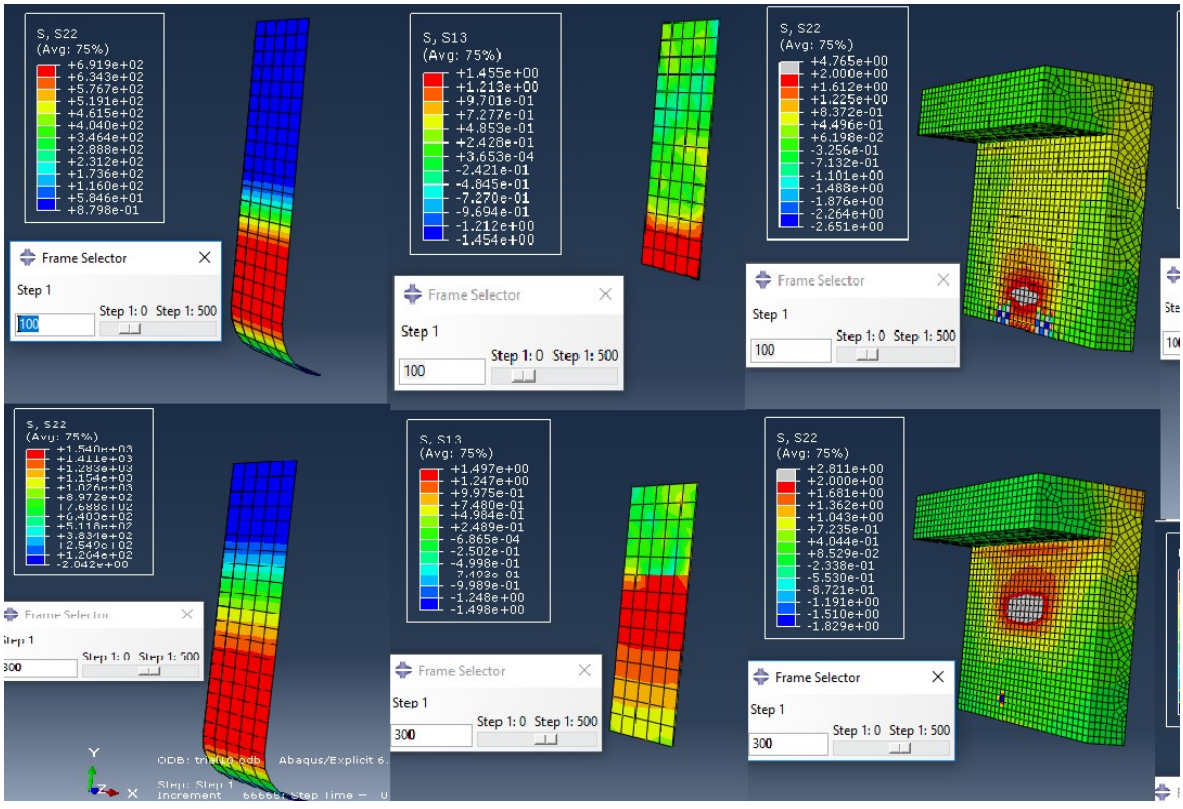

Fig. 17. State of stress for the FRP strip, the cohesive interface and the concrete block when the FRP strip is simply bonded to the unit T-beam.

4.3 Numerical simulation of the anchored FRP strips

This time apart from the numerical simulation of the cohesive interface the actual anchoring detail that was employed in specimens shown in figure 3c was numerically simulated. This was done by numerically simulating the steel anchor bolts, the corresponding holes in the concrete volume as well as the steel plate that these bolts were attached to together with the

upper part of the FRP strip. The same loading sequence and support conditions described before were also employed here. Figure 18, depicts the comparison of the measured capacity of a unit T-beam specimen with FRP strips with and without anchors with the corresponding numerical predictions. As can be seen in this figure, the numerical predicted capacity is in good agreement with the corresponding measured maximum value. Moreover, it can also be seen that the numerically predicted behaviour simulates successfully the observed increase in deformation capability of such a connection as the brittle debonding mode of failure is avoided; instead, the prevailing mode of failure is either the fracture of the FRP strip or the failure of parts of the anchoring scheme itself (see section 2.2). Figure 19 depicts the state of stress for the FRP strip during the loading process. The upper far left part of this figure is at the beginning of the loading sequence whereas the lower far right part is at the end of the loading sequence when the maximum capacity of this connection was reached.

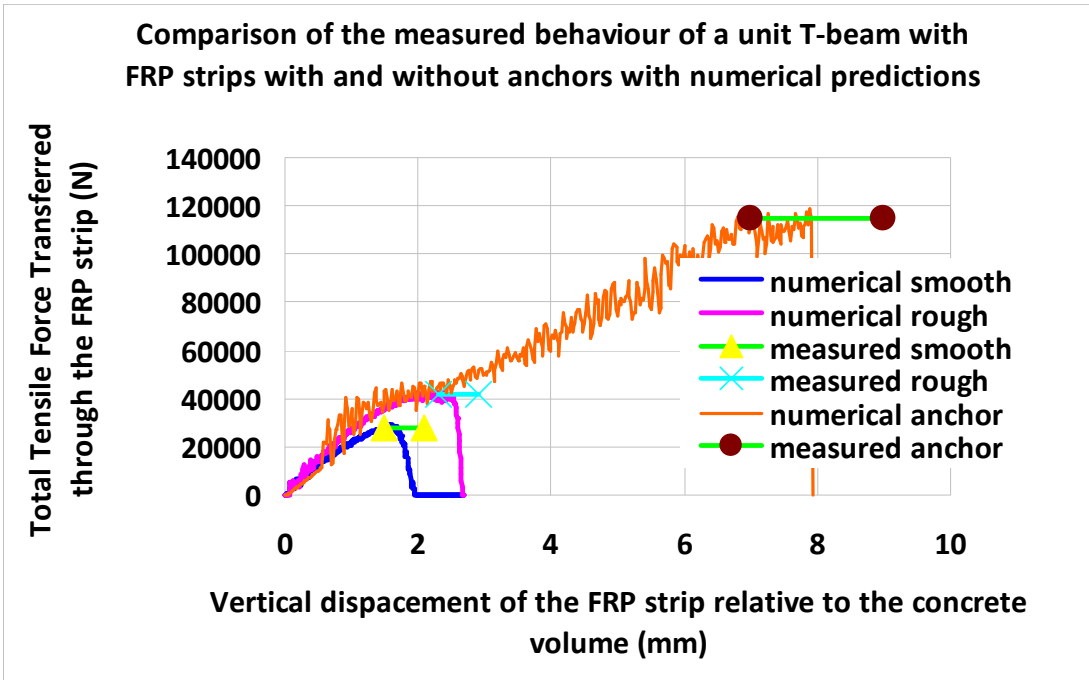

Fig. 18. Comparison of the measured capacity of a unit T-beam specimen with FRP strips with and without anchors with numerical predictions

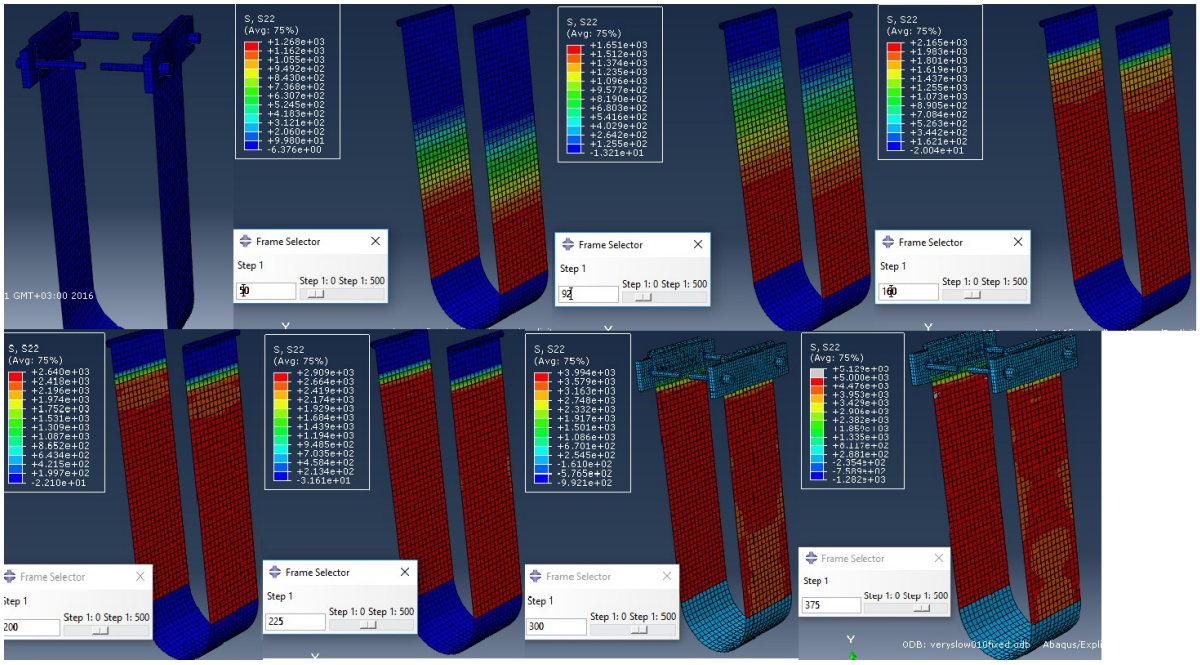

Fig. 19. State of stress Fig. 19. State of stress for the FRP strip during the loading process.

The plots in between these two far parts in figure 19 depict the state of stress of the FRP in consecutive stages from the beginning till the end of the loading process, as they were predicted from the employed numerical simulation. Figure 20, depicts the state of stress of the concrete block for a unit T-beam specimen having the FRP strip anchored following the fashion in portraying the loading sequence which was previously described for figure 19. As can be seen in the upper part of figure 19, the FRP strip transfers initially its force to the concrete volume through the cohesive interface utilizing the bond mechanism, as described in section 4.2. The same is also observed at the upper part of figure 20. When this bond capacity is exceeded the debonding failure occurs. From this stage onwards the transfer of force relies solely on the successful anchoring system as can be seen in the lower parts of figures 19 and 20. This mechanism has been studied in section 2.3. and has been investigated in detail in previous publications. From these numerical predictions it is demonstrated that the employed numerical simulation was successful realistic approximations of the studied transfer of force mechanisms from the FRP strip to the concrete block including both the bond and the achoring mechanisms.

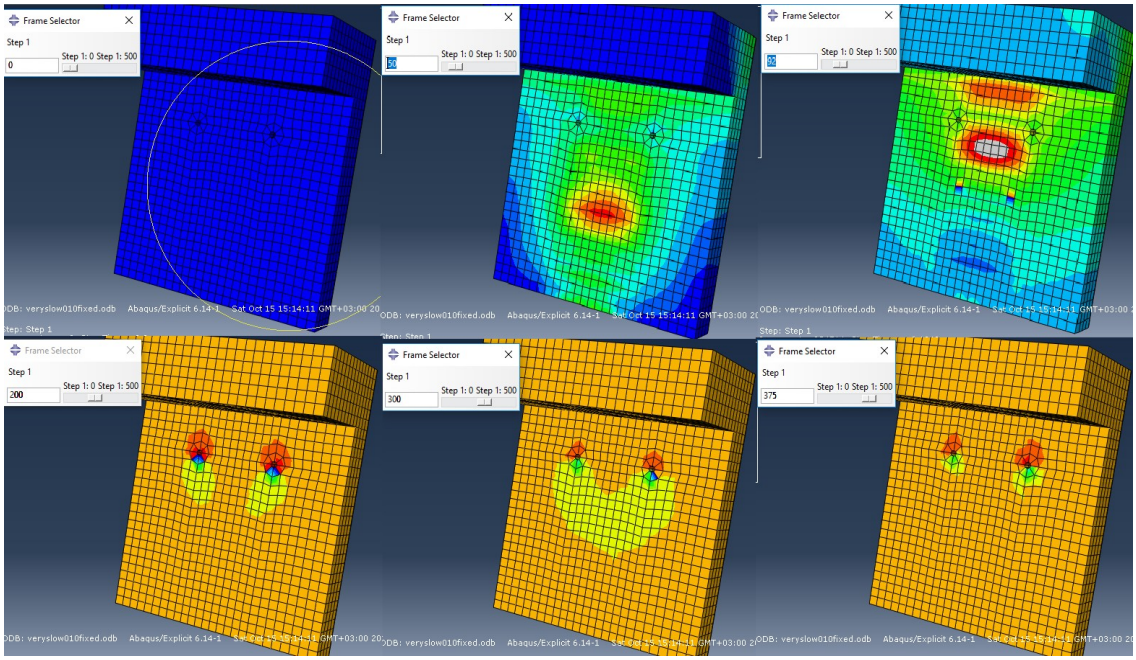

Fig. 19. State of stress for the concrete block of the unit T-beam during the loading process when the FRP strip is anchored.

5 CONCLUSIONS

1. The behaviour of anchoring techniques for carbon open hoop FRP strips utilized as external shear reinforcement for R/C T-Beams was studied experimentally employing the relatively simple loading arrangement of "unit T-Beam" specimens. It was demonstrated that the anchoring scheme devised by the authors [3] can provide the required satisfactory transfer of forces between the FRP strip and the concrete volume of the T-Beam.
2. The special treatment of the bond surface resulted, as expected, in a considerable increase in the level of the maximum axial load that can be transferred from the unanchored CFRP strip to the concrete volume through the bond surface. On the contrary, in the case of employing the efficient anchoring scheme, devised by the authors, the influence of the bond surface is immaterial. This is because in this case the transfer of tensile forces between the FRP strip and the concrete volume of the T-Beam at limit state is achieved solely through the used anchoring scheme. The debonding of the FRP strip already occurs at a preceding stage.
3. The applicability of the anchoring scheme devised by the authors to successfully inhibit the debonding mode of failure for such open hoop CFRP strips employed in shear strengthening of R/C T-Beams was further demonstrated in the laboratory employing for this purpose a prototype R/C T-Beam specimen. An alternative anchoring scheme [10] that was investigated also seems promising.
4. The numerical simulation of the behaviour of FRP strips simply bonded to the concrete surface of the unit T-beam specimens was successful to predict the state of stress that develops at the FRP strip, at the cohesive interface and at the concrete block during the various stages of the loading sequence, as they were observed during testing, till the debonding failure. From the comparison of the numerical predictions with the measured capacity it can be concluded that tt is non-conservative to base the estimate of the bearing capacity of bonded FRP strips on concrete surface on the direct tensile strength of concrete, unless the contact surface of the concrete is properly treated prior to bonding the FRP strips. Moreover, because the debond-

ing mode of failure leads to a brittle respond is wiser to adopt a higher value of safety factor than it is the case of anchored FRP strips.
5. From the presented numerical predictions it is demonstrated that the employed numerical simulation was successful in obtaining realistic approximations of the developing transfer of force mechanisms from the FRP strip to the concrete block including both the bond and the anchoring mechanisms.

ACKNOWLEDGEMENTS

Carbon fibers, anchors and epoxy resins were provided by Sika Hellas. One of the anchoring devices employed in this study is patented under the no. EP09386037.7 Partial financial support for this investigation was provided by the Hellenic Earthquake Planning and Protection Organization.

- To the memory of Ray W. Clough, Professor Emeritus of the University of California, at Berkeley, U.S.A.

REFERENCES

[1] Bakis, et al., (2002) Fiber-Reinforced Polymer Composites for Construction - State of the Art Review', Journal of Composites of Construction, ASCE, May 2002.
[2] Lu XZ, Teng JG, Yea LP, Jiang JJ. (2005) Bond–slip models for FRP sheets/plates bonded to concrete. Journal of Engineering Structures 2005;27:920–37.
[3] Manos GC, Katakalos K, Kourtides V. (2011) Construction structure with strengthening device and method. European Patent Office, Patent Number WO2011073696 (A1); 2011 (23.06.11).
[4] Manos GC, (2011) Consequences on the urban environment in Greece related to the recent intense earthquake activity", Int. Journal of Civil Engineering and Architecture, Volume 5, No. 12 (Serial No. 49), pp. 1065–1090.
[5] Manos GC, Katakalos K, Kourtides V. (2012) Cyclic behaviour of a hybrid anchoring device enhancing the flexural capacity and ductility of an R/C bridge-type pier strengthened with CFRP sheets., Journal of Civil Engineering Research 2012, 2(6): 73-83, DOI: 10.5923/j.jce.20120206.04.
[6] Manos GC, Katakalos K., (2012) Enhanced Repair and Strengthening of Reinforced Concrete Beams Utilizing External Fiber Reinforced Polymer Sheets and Novel Anchoring Devices, 15WCEE, Portugal.
[7] Manos GC, Katakalos, K. (2013) Investigation of the Force Transfer Mechanisms for Open Hoop FRP Strips Bonded on R/C Beams with or without Anchoring Devices", Open J. Civil Eng., September 2013, Vol.3, No.3, pp, 143-153.
[8] Manos GC, Katakalos K. (2013) The use of fiber reinforced plastic for the repair and strengthening of existing reinforced concrete structural elements damaged by earthquakes, Editor M. Masuelli, 2013, ISBN: 978-953-51-0938-9
[9] Manos G.C., Theofanous M., Katakalos K. (2014) Numerical simulation of the shear behaviour of reinforced concrete rectangular beam specimens with or without FRP-strip shear reinforcement, J. Advances in Engineering Software Vol. 67, pp. 47-56, 31-1-2014.

[10] Manos GC and Katakalos K (2015) Experimental investigation of concrete prismatic specimens, strengthened with CFRP strips and FRP anchorage, under tensile loading, Technical Report to Sika Hellas
[11] Manos GC and Katakalos K, Kourtidis V. (2017) "Novel Anchoring Devices for Open Hoop Fiber Reinforcing Polymer Strips used in the Shear Upgrade of R/C T-Beams", World Conference on Earthquake Engineering, 16WCEE 2, Santiago, Chile.
[12] Wu Y, Zhou Z, Yang Q, Chen W. (2010) On shear bond strength of FRP-concrete structures. Journal of Engineering Structures 2010;32:897–905.
[13] Hibbitt, Karlsson & Sorensen, 2010, Inc. ABAQUS user's manual volumes I-V and ABAQUS CAE manual. Version 6.10.1. (Pawtucket, USA).